Mooring line fatigue damage evaluation for floating marine energy converters: Field measurements and prediction

Philipp R. Thies*, Lars Johanning, Violette Harnois, Helen C. Smith, David N. Parish

CEMPS - College of Engineering, Mathematics and Physical Science
Renewable energy research group, University of Exeter
Penryn Campus, Trelievver Rd, Penryn, TR10 9EZ, UK

Abstract

The vision of large-scale commercial arrays of floating marine energy converters (MECs) necessitates the robust, yet cost-effective engineering of devices. Given the continuous environmental loading, fatigue has been identified as one of the key engineering challenges. In particular the mooring system which warrants the station-keeping of such devices is subject to highly cyclic, non-linear load conditions, mainly induced by the incident waves.

To ensure the integrity of the mooring system the lifecycle fatigue spectrum must be predicted in order to compare the expected fatigue damage against the design limits. The fatigue design of components is commonly assessed through numerical modelling of representative load cases. However, for new applications such as floating marine energy converters numerical models are often scantily validated.

This paper describes an approach where load measurements from large-scale field trials at the South West Mooring Testing Facility (SWMTF) are used to calculate and predict the fatigue damage. The described procedure

*corresponding author, Tel.: +44 (0)1326 371821, Fax: +44 (0)1326 254243
Email address: P.R.Thies@exeter.ac.uk (Philipp R. Thies*)

employs a Rainflow cycle analysis in conjunction with the Pålmgren-Miner rule to estimate the accumulated damage for the deployment periods and individual sea states.

This approach allows an accurate fatigue assessment and prediction of mooring lines at a design stage, where field trial load measurements and wave climate information of potential installation sites are available. The mooring design can thus be optimised regarding its fatigue life and costly safety factors can be reduced. The proposed method also assists in monitoring and assessing the fatigue life during deployment periods.

Keywords:

wave energy converter, rainflow cycle, reliability, dynamic load, load measurements, field test, mooring line, fatigue prediction

---

Contents

1. Introduction

The development of wave and tidal energy so far has been confined to the installation of prototypes and small-scale demonstration projects. However, the significant potential of these marine renewable energy technologies becomes apparent through recent activities. In the UK, the Crown Estate has leased marine energy sites for large commercial-scale developments with a total capacity of 1.6GW. The 11 projects in the Pentland Firth and Orkney waters are expected to be installed during 2014-2020. An installed capacity in the order of 400MW is anticipated for floating wave energy applications (BVG Associates, 2011).

On the pathway towards commercial deployments, field tests are an indispensable stepping stone. They must demonstrate the installation and operation procedures and must assess the performance and load behaviour. Consequently, marine energy technologies are being increasingly field tested. Several test centres aim to bridge the gap between lab-based prototype devices and full-scale field deployment with several field test sites around the world (Mueller et al., 2010). The available sites may be broadly distinguished regarding the type and scale of device that may be tested.

Table 1 provides a non-exhaustive list of field test sites devoted to the deployment of marine energy converters (MECs) ranging from small scale, so called nursery sites, to full scale commercial demonstration projects, such as the Wave Hub. The increasing number and use of field test sites will provide a growing amount of valuable field data of energy yield performance and component load information. Energy yield data will directly inform the economic models while the load behaviour contains valuable indications for the long-term reliability of devices.

This paper focuses on load information for mooring systems of floating wave energy converters. The mooring system for these applications requires careful design and assessment, as proven solutions in the oil and gas industry cannot simply be adopted. The differences of installation location, mooring arrangement, motion requirements and physical size result in considerably different coupled response and load characteristics. These affect the accumulated cyclic loading due to non-linear mooring line behaviour and reduce the capacity of components to withstand ultimate dynamic loadings, as discussed by Johanning et al. (2005, 2006, 2007).

It is estimated that moorings incur about 10% of the capital cost for a MEC installation (Dalton et al., 2012). Therefore the use of high safety factors would mean a potential over-design and the risk of non-viable economics. The research challenge is to develop a thorough understanding of mooring system behaviour in real wave, wind, current and tidal conditions and robust design procedures that allow the design of reliable, yet economic mooring systems. This paper presents an analysis of mooring field measurements which aims to advance the understanding of expected mooring fatigue performance in floating marine energy applications. A method to determine the fatigue damage for individual sea states and to subsequently predict the accumulated fatigue damage is proposed and demonstrated. The engineering application of this approach is twofold. In early design stages, it provides an improved fatigue life estimate for MEC components which encourages leaner designs. During deployment, the accrued fatigue damage of components can be monitored and assessed to ensure the fatigue capacity remains sufficient, or to inform the scheduling of required maintenance.

Table 1: Marine renewable energy field test sites

Name	Location	Capacity	Scale	Installation	Reference
Wave energy test sites					
Wave Hub	Cornwall, UK	4 berths, 20MW	Full scale	Deployment planned 2013	SWRDA (2011)
Falmouth Bay test site	Cornwall, UK	3 MW	Scaled & full scale	Operational	FaB Test (2011)
South West Mooring Test facility	Cornwall, UK	1 berth	$\frac{1}{3}$ scale	Operational	Johanning et al. (2011)
EMEC Billia Croo	Orkney, Scotland	5 berths, 2.2MW	Full scale	7 installations since 2004	EMEC (2011a)
EMEC Scapa Flow	Orkney, Scotland	1 berth 75 kW	Nursery site	under development	EMEC (2011b)
Galway Bay Test site	Ireland	1 berth	$\frac{1}{3} - \frac{1}{5}$ scale	2 installations	Mueller et al. (2010)
Nissum Bredning	Denmark	1 berth	$\frac{1}{4}$ scale	>30 tests	Mueller et al. (2010)
DanWEC Roshage Pier	Hanstholm, Denmark	Pier access	Full scale	2 installations	Mora-Figueroa et al. (2012)
Lysekil test site	Sweden	10 berths, 10kW	Small scale	Array of 10 installed	Leijon et al. (2008)
SEMREV	Le Croisic, France	3 berths, 2.5MW	Full scale	Operational	Mouslim et al. (2009)
Portuguese Pilot Zone	Fig. de Foz, Portugal	80MW	Full scale	Operational	Palha et al. (2010)
Runde Marine Energy Test Centre	Runde, Norway		Medium Scale	2 installations	Mora-Figueroa et al. (2012)
BIMEP	Basque Country, Spain	4 berths	Full scale	under development	Mora-Figueroa et al. (2012)
Plocan	Canary Islands, Spain	6 berths	Full scale	under development	Mora-Figueroa et al. (2012)
Agucadoura	Portugal	3 berths	Full Scale	3 installations	Mora-Figueroa et al. (2012)
Peniche test site	Portugal	Medium scale	Medium Scale	3 berths, 300kW	Mora-Figueroa et al. (2012)
Atlantic Marine Energy Test Site (AMETS)	Belmullet, Ireland	Full scale	4 berths	Under development	Mora-Figueroa et al. (2012)
NNMREC Ocean Test Berth	Oregon, USA	5 berths	Full scale	Operational	Mueller et al. (2010)
HWMREC Kaneohe test site,	Hawaii, USA	2 berths	Medium scale	1 installation, plans for 4 berths, 2MW	Mueller et al. (2010)
Tidal energy test sites					
EMEC Fall of Warness	Orkney, Scotland	7 berths, 5MW	Full scale	8 installations since 2007	EMEC (2011a)
EMEC Shapinsay Sound	Orkney, Scotland	1 berth, 75 kW	Nursery site	under development	EMEC (2011b)
FORCE test site	Nova Scotia, Canada	3 berths, 5MW	Full scale	3 installations	FORCE (2012)

The remainder of the paper comprises three main parts. Section 2 briefly outlines the arrangements of the field experiments and the treatment of collected load data. Section 3 describes the general methodology employed to analyse and predict the fatigue damage, while section 4 presents the results for the individual sea states and long-term prediction, both of which are discussed in section 5. The paper concludes in section 6 with the wider implications to floating MECs that can be drawn from the study.

2. Mooring field trials

2.1. South West Mooring Test Facility

The South West Mooring Test Facility (SWMTF) is a unique large scale installation designed to investigate the mooring load and response in real sea conditions. It consists of a generic 3.25t buoy that can be variably moored and has been installed with a three-leg catenary hybrid (rope-chain) mooring since March 2010. It is located at a relatively sheltered site in the southwest part of Falmouth Bay, Cornwall, UK (see fig. 1), in a water depth of 27m (low tide mark) and tidal variations of up to 5.4m. The mean wave power in Falmouth Bay, calculated from a hindcast model run over a period from 1989 to 2011, is 5 kW/m (van Nieuwkoop et al., 2013). A design schematic of the buoy and a picture during installation is shown in fig. 2. The dimensions of the floating buoy, the mooring arrangement and the instrumentation are briefly described in the following.

The main components of the SWMTF are a cylindrical steel support structure, a floating body manufactured from foam elastomer and a lantern structure. Figure 2(a) presents a schematic drawing of the buoy with its

Table 2: Structural properties of South West Mooring Test Facility (SWMTF) Buoy and Mooring arrangement

Buoy		Mooring	
Mass	3250 kg	Anchor	1.1 tonne drag embedment
Draft	1658 mm	5m ground chain	32mm stud link
Diameter floating body	2900 mm	36m riser chain	24mm open link
Diameter central column	355 mm	20m rope tail	44mm jacketed parallel lay nylon
Radius of gyration	$x = y = 576$mm $z = 744$mm		

lantern and attached instrumentations and the main properties are listed in table 2. The structural integrity is provided by the central support structure that provides the fixing points for the floating body, the lantern and the load cells, which provide the attachment points to the mooring lines.

The chosen mooring arrangement is a three-leg hybrid chain-nylon rope catenary assembly, comprising a 5m ground chain, 36m riser chain and 20m rope tail as specified in table 2. The mooring lines are spread equally at 120° and anchored on the seabed with three embedment anchors at a diameter of 80m. A plan view of the mooring arrangement is shown in fig. 3.

The buoy is extensively instrumented to acquire data regarding the buoy's position, motion response and the associated mooring line loads, as well as the wind velocity. In addition, an Acoustic Doppler systems (ADCP) is installed in close vicinity to record the environmental influences, such as

Table 3: Summary of main SWMTF sensors

Parameter	Sensor	Sample frequency [Hz]	Signals
Wave elevation	Teledyne RDI Workhorse Waves Array Acoustic Doppler system	2	4
Buoy Response	Multi axis inertial, MotionPack	20	6
Mooring load	In-line load cell	20	3
Wind	WindSonic	4	digital
Tidal current	Aanderaa DCS 4100R velocity meter	10s averages	digital
Position	Global Positioning System (GPS)	10	digital

incident waves and tidal currents, see table 3. This paper draws on the mooring line load data and the incident wave elevation data.

2.2. Deployment, data validation and correction

While the SWMTF has been collecting load information since March 2010, the period where the incident wave elevation was also measured is limited to nine months from 16 September 2010 - 07 June 2011. This determined the time period for the analysis presented in this paper. The load data was sampled at 20Hz and stored in individual 10 minute files. The subsequent mean values of each file are depicted in fig. 4(a).

The mean loads in line 1 and 2 are similar which is expected in a balanced mooring system. There is a distinct drift in the measured loads for line 3

until the load cell became saturated. Additionally a sudden decrease in the loads of line 1 and 2 is observed at the end of January which was attributed in Harnois et al. (2012) to a dragging event of anchor 3, creating a new equilibrium of the mooring system. After this initial quality control of the data, the load data for mooring line 3 was corrected in four steps. Firstly the data after the saturation point of the load cell was removed. Secondly, a moving average with a window size of 3000 data points, is calculated for the load in line 3 and subtracted from the initial measurements. The average value of the mean load in line 1 and 2 is added to the detrended load data of line 3, because a similar load is expected in each mooring line of a balanced mooring system. The corrected load data is shown in fig. 4(b). Any subsequent analysis of the time series for line 3 demeans the raw data series and adds the corrected mean value.

A point to emphasise is the relatively high sampling frequency (20 Hz) of the mooring line loads. This was chosen deliberately to accurately capture the peak mooring loads. An assessment to what extent the sampling frequency improves the accuracy of the measured mooring line load is presented in Harnois et al. (under review), which yields an improved capture of peak loads through at higher sampling frequencies. A sampling frequency of 20Hz improves the capture of the peak mooring line load by about 8% for the recorded peak loads, compared to a 2Hz sampling frequency. This improved capture of peak loads is important for fatigue estimates, as any load uncertainties translate exponentially into the required fatigue life safety factor, as discussed in sec. 5.2.

3. Methodology for fatigue load analysis and prediction

Fatigue is a well-known failure mechanism for materials and components that are exposed to fluctuating load conditions (Schütz, 1996). Floating MECs are particularly subject to dynamic and cyclic loading as they are most effective in locations with high wave energy densities and often depend on the wave-induced motion for power-take-off purposes.

Two distinct approaches have evolved to evaluate fatigue reliability (Cui, 2002; Schijve, 2009):

1. Stress-life cumulative damage models (S-N approach) - methodology to predict fatigue life, considering the cumulative fatigue damage, where a failure occurs after a number of loading cycles N, at a particular stress range S.
2. Fatigue crack growth models (fracture mechanics approach) - examining the fracture behaviour of mechanical elements under dynamic loading, where failures occur if dominant cracks have grown to a critical length where the remaining strength of the component is insufficient.

The S-N approach is based on the linear damage accumulation assumption (Pålmgren-Miner rule). It does not consider the load sequence, which influences the crack growth behaviour in the elastic-plastic fracture regime and during micro-structurally small crack growth. As such, the fracture mechanics approach would yield a more accurate fatigue life prediction (Cui, 2002). However, at present fatigue crack growth models are not the dominant method used for fatigue design in industry because the required crack growth rate is not readily available and the initial crack size is not always known. Nijssen (2006) concludes in a detailed comparison of fatigue prediction methods for wind turbine blades that the experimental

and computational effort to carry out a fracture mechanics cycle by cycle approach is not justified by the small advantage over Miner's rule. The present paper aims to estimate the fatigue life for mooring lines and uses the cumulative damage models.

S-N curves describe the fatigue properties of different materials. These curves are found empirically through fatigue tests and show the number of cycles to failure N, as a function of the cyclic stress S. Fatigue curves are modelled with a power law, that stems from the linear regression of fatigue test results. The number of cycles $N(S)$ to failure for a particular cyclic stress range S is described by Equ.1.

$$N(S) = KS^{-\beta} \tag{1}$$

$$log\,(N(S)) = log\,(K) - \beta \cdot log\,(S) \tag{2}$$

Where $N(S)$ is the number of cycles at a certain stress, S is the constant amplitude cyclic stress, K is the intercept parameter of the S-N curve and β describes the slope of the S-N curve.

Fatigue damage is a nonlinear function of the stress amplitude (comp. equation 3) which implies that uncertainties in the load response are amplified, leading to large uncertainties in the fatigue damage evaluation. Marine energy converters are subject to irregular, dynamic wave forces and the load response in the field is subject to uncertainties. The mooring system restraints the motion of the floating devices, yet has to be compliant enough to allow the motion for energy conversion. The load response of different mooring configurations for floating MECs is being researched

(Johanning et al., 2006, 2007; Fitzgerald and Bergdahl, 2008) but conditions of field deployment still carry considerable uncertainties. As a result the MEC mooring designs have a tendency to be overly conservative and costly in order to accommodate the load uncertainties. This is an issue for both extreme load and fatigue design. While the extreme loads for different environmental conditions are discussed in Harnois et al. (under review), this paper presents the methodology and results to estimate and predict the mooring line fatigue damage for floating MECS on the basis of field measurements.

3.1. Rainflow cycle method

For load cycles of randomly varying amplitude the so-called rainflow count method is commonly used to evaluate fatigue damage, as it realistically considers the fatigue damage caused by each individual load cycle. It identifies and counts the stress ranges corresponding to individual hysteresis loops of the component material. The mooring force varies with wave elevation and the subsequent motion response of the floating device. As waves can be described as a random process the rainflow cycle count methodology is used here.

The rainflow algorithm is based on the definition for a rainflow cycle of Rychlik (1987), see fig.5. Starting from a local load maximum Max_K two minima are identified before and after Max_K, i.e. Min_{K-} and Min_{K+}. The point with the smaller deviation from Max_K is chosen as the rainflow minimum $Min_{K,RFC}$, giving the k:th rainflow cycle $(Min_{K,RFC}, Max_K)$. This algorithm is then repeated over the entire time series t.

Further, with t_K as the time of the k:th local maximum and the rainflow

amplitude $S_{k,RFC}$ the total damage $D(t)$ can be calculated by the Pålmgren-Miner rule. It is also known as the linear cumulative fatigue damage rule and assumes that the each load cycle causes a damage of $1/N(S_{k,RFC})$. Using this linear cumulative rule, a failure occurs if $D \geq 1$. The fatigue damage $D(t)$ is calculated as the sum of the individual load amplitudes:

$$D(t) = \sum_{t_k \leq t} \frac{1}{N(S_{K,RFC})} = \frac{1}{K} \sum_{t_k \leq t} (S_{k,RFC})^{\beta} \tag{3}$$

where $N(S_{k,RFC})$ is the number of cycles during the time t and $S_{k,RFC}$ denotes the stress amplitudes established in the rainflow cycle count. K and β describe the fatigue behaviour of the material or component through the shape of the S-N curve, where K denotes the intercept and β the slope of the curve, i.e.:

$$N(S) = \begin{cases} K \cdot S^{-\beta} & S > S_{\infty} \\ \infty & S \leq S_{\infty} \end{cases} \tag{4}$$

with $N(S)$ number of load cycles; S stress amplitudes; S_{∞} fatigue limit

For the mooring materials considered later, β is in the range from 3 to 5. Therefore, following equ.3, a doubling of the load amplitude leads to an increase of fatigue damage by a factor of between 8 and 32. Hence, the fatigue damage for a given material is largely dependent on the largest load cycles and to a lesser extent dependent on the occurrence of cycles.

3.2. Cycle count and damage estimation

The rainflow cycle analysis of the mooring tensions has been carried out with the Matlab toolbox developed by the WAFO-group (2000). The field data was processed in blocks of three hours to allow a meaningful estimation of the prevailing sea states. The calculation comprises two subsequent steps for each measured load time history:

1. Rainflow cycle count to compute rainflow matrix (RFM), showing the amount of load cycles for different stress ranges.
2. Fatigue damage calculation, which computes the accumulated damage, based on the RFM and the fatigue properties of the mooring line.

The rainflow matrix shows the number of load cycles for a given load range interval [Min, Max]. The number of occurrence indicates the number of observed load cycles in the specific load range. Additionally a rainflow filter is used to reduce signal noise by excluding load cycles with a tension force $F \leq 200N$ which contribute a negligible amount of fatigue damage. The chosen discretisation level n for the RFM analysis is $n = 40$ which strikes a reasonable balance between resolution detail and sufficient bin population. The generated RFM forms the basis of the fatigue damage calculation, as defined by the Pålmgren-Miner rule in equ. 3. This analysis is repeated for each of the three hour blocks which are then grouped according to the prevailing sea states.

The filtered rainflow matrix for mooring line 2 in a moderate sea state is shown in fig. 6. The load cycles in the upper left corner have the largest amplitudes and will thus result in the largest fatigue damage.

3.3. Mooring line fatigue characteristics

The two primary factors to affect fatigue reliability are the material's fatigue strength and the applied cyclic loading. While the fatigue strength is an intrinsic material and mechanical characteristic, the applied loading describes an extrinsic process. Two approaches are common to evaluate a material's fatigue reliability (Wang et al., 1997). The crack growth model examines the fracture behaviour of mechanical elements under dynamic loading, where failures occur if dominant cracks have grown to a critical length. The

stress-life (S-N) approach considers the cumulative fatigue damage, where a failure occurs after a number of loading cycles N, at a particular stress range S. The fatigue life design for offshore structures is commonly based on the use of experimentally determined S-N curves (Stacey and Sharp, 2007), which are also used in the present analysis. S-N fatigue curves are modelled with a power law (equ.5), that stems from the linear regression of fatigue test results (equ. 6).

$$N(S) = KS^{-\beta} \tag{5}$$

$$log\,(N(S)) = log\,(K) - \beta \cdot log\,(S) \tag{6}$$

The parameters for design S-N curves for tension-tension fatigue of the component material at question are readily found in design standards. The mooring line materials considered here are given in DNV-OS-E301 (2010) and are plotted in fig. 7. The graph shows the reference fatigue design curves for steel wire ropes and chain. The given curves imply that the chain is exposed to the corrosive influence of seawater, while the curves for steel wire rope assume corrosive protection, e.g. through outer sheath lining. From the four mooring types, spiral steel wire rope has the most favourable fatigue properties followed by the stranded wire, the studded- and the studless chain.

As the S-N curves are given in terms of the nominal stress range, the measured tension load signal must be converted to a nominal stress using:

$$\sigma_{NOM} = \frac{F_{Moor}}{A} \tag{7}$$

σ_{NOM} is the nominal stress [MPa], F_{Moor} is the measured mooring force [N] and A is the cross-sectional area of the mooring line [mm^2].

3.4. Estimation of annual load conditions

With the above procedure, the fatigue load conditions can be readily assessed for the individual sea states. Some additional information and subsequent calculations are needed to generate an annual load spectrum from the individual sea states. Firstly, the annual wave characteristics of the deployment site are required. As a second step, the probability of each sea state is assigned to the estimated fatigue damage of each sea state. The objective is to derive a multiplicative factor for each individual sea state, in order to estimate the annual accumulated fatigue damage. This is found to be:

$$D_{annual}(H_s, T_p) \mapsto D_{measured}(H_s, T_p) \cdot M \tag{8}$$

where $D_{annual}(H_s, T_p)$ is the annual accumulated fatigue damage for a given sea state at the site (specified through H_s and T_p), $D_{measured}(H_s, T_p)$ is the calculated fatigue damage based on the measured load data and M is the adjusting multiplying factor, given by:

$$M = P_{assign}(H_s, T_p) \cdot 8760h \cdot \frac{1}{3h} \tag{9}$$

$P_{assign}(H_s, T_p)$ is the assigned annual probability, effectively the sum of $P_{site}(H_s, T_p)$ assigned to a measured sea state. The factors relate to the number of hours for a year (8760h) and account for the fact that the fatigue damage D is calculated for 3 hour intervals.

One difficulty that is likely to arise here is that the measured tests do not coincide with the sea states expected at the site, for example by means of a long-term hindcast. How well the conditions during measurement and the long-term statistical distribution coincide must be evaluated on a site and

case specific basis. Two ways of dealing with a discrepancy of environmental conditions are suggested here which are representative of the situation encountered in practice where both modelled data and measured wave data may be available:

1. Observed wave climate: Only the measured conditions are considered. If sufficient data is available the observed wave climate may be normalised to a full year. Thus, the assumption is that the measured time is representative of an entire year and that the year is representative of long-term conditions. If the data is deemed not to be sufficient to represent an entire year, the fractional year could be calculated.
2. Modelled long-term wave climate: The wave environment determined through a hindcast model is used for the fatigue estimate.

The first approach adheres to the available data and thus yields a robust estimate for the available field data. However, it usually does not account for inter-annual variations, where the mean wave climate of a long-term hindcast would be more appropriate. When the data is only suitable to estimate the fatigue damage for a fraction of the year, additional measurements or alternatively experimental or numerical modelling should be carried out to supplement the number of load cases.

4. Results

In this section the key results of the fatigue analysis and prediction for the field measurements at the SWMTF site are presented. Firstly the wave climate parameters during the deployment period are compared with those estimated through an eight-year wave hindcast model. Subsequently the fatigue damage for the individual sea states is presented for the 24mm open

link top chain for each of the three mooring lines. Based on these damage characteristics the fatigue life is predicted.

The presented methodology can be equally applied to other sections of the mooring line, including the connectors. However, S-N curves are most readily available for standard mooring lines and thus they have been chosen for the case study. The fatigue life of the mooring line is governed by the weakest link, which is not necessary the chain. However, the highest and most dynamic forces are expected at the top end of the mooring line, so a fatigue analysis of the riser chain was selected for this paper.

4.1. Wave climate parameters

The wave climate comparison between field measurements and long-term conditions is of importance to judge how representative the field measurements are for the expected long-term exposure of the device. For the present case the measured conditions are representative as almost all expected wave heights and periods are covered. However some distinctions with regard to the wave parameters are made in the following.

During the deployment period for the presented analysis the SWMTF was subjected to a total of 23 different sea states (classified in bins of 0.5m significant wave height,H_s, and 2 second wave peak period, T_p) over a period of 5,976hours. The percentage contribution of the individual sea states is shown in fig. 8(a). It can be seen that the majority of the time a low sea state with $H_s \leq 1m$; $T_p = 4-8s$ prevailed, reflecting the sheltered character of the site, but larger sea states up to $H_s = 3$m also occurred. During the initial site assessment, a hindcast wave model for the period from March 2000 to November 2008 was run using the SWAN nearshore wave model. SWAN

is a spectral wave model designed for the propagation of sea states in the nearshore region, accounting for nearshore processes and energy dissipation. The model was run over a 200m resolution bathymetry grid, across a 33 x 30.6 km domain with open water boundaries along two sides. Three-hourly offshore wave parameter data (significant wave height, mean period and mean direction) at four grid points from the Met Office UK Waters Model (Golding, 1983) were used as input for the model, and constant wind field parameters, also from the Met Office, were applied across the model domain.

Over the 8.5 year period for which the hindcast was run, no recorded data were available within the model domain for calibration and validation studies. However, an ADCP was deployed at the SWMTF site in September 2010 and recorded approximately five weeks of wave parameters. A second SWAN model was established to run a validation hindcast for this period over a similar domain, but using input data from the Met Office Wavewatch III North Atlantic European model which replaced the UK Waters Model in 2008. Comparisons between the model and the ADCP data can be seen in fig. 9.

The results of the validation study illustrate the challenges inherent in using a model such as SWAN in such a sheltered location. While SWAN generally represents the wave heights well, although at times over-predicting larger waves, there are two particular aspects to note in the wave period predictions. Firstly, there is a consistent under-estimation of mean period by the model, and secondly, the model appears unable to represent the very small long-period swell occurring in the early stages of the record. This has been attributed in van Nieuwkoop et al. (2013) to the sheltered position of the site, exposing the difficulties of fully modelling the swell refraction. A method to account for this error is discussed in section 4.3.

Table 4: Comparison of measured and modelled wave parameter estimates for SWMTF site

	H_s [m]		T_p [s]	
	Mean	Median	Mean	Median
Measured	1.2	1.0	7.3	6.1
Hindcast	1.4	1.3	5.2	3.9
Difference	-0.2	-0.3	2.1	2.2

Based on the 8.5-year model results, the relative contribution of sea states is depicted as a scatter plot in fig. 8(b). When comparing the hindcast against the measured scatter plot the distribution of wave heights is very similar, while the wave periods seem to be under-predicted in the numerical model, as predicted by the validation study (10). The measured wave heights are slightly smaller than the modelled distribution, with 18% more occurrence of $H_s = 0 - 0.5$m and no occurrence of Hs ¿ 3m. With regard to the wave periods, Tp, the distribution appears to be shifted by 2s towards the lower periods for the numerical model. The mean values are specified in the distribution plots and are summarised together with the median values in table 4, confirming that the modelled wave climate has a slightly smaller mean H_s while the mean and median T_p are more than 2 seconds below the measured values. An aspect which the model seems to miss is the situation of small, long period swells with $T_p \geq 12$s, as discussed above.

4.2. Damage for individual sea states

From the three-hourly fatigue estimates a mean fatigue damage for the 23 individual sea states is calculated to characterise the fatigue behaviour

of the separate mooring lines. Figures 11-13 show the mean accumulated fatigue damage for the observed sea states. The damage is plotted on a logarithmic scale which is consistent for the three mooring lines to allow a direct comparison.

A general observation which can be made is that the fatigue damage appears to be directly proportional to wave height, $D \propto H_s$, and inversely proportional to wave period $D \propto \frac{1}{T_p}$. As such, the fatigue damage increases with increased wave heights and decreases for larger wave periods T_p for a given wave height. The dominant fatigue driver for the measured loads is the wave height which increases the fatigue damage by up to a factor of 10^4, while the wave period changes the damage D by a factor of up to 10^2. This is largely consistent across all measured sea states.

A comparison between the three mooring lines shows that line 3 is subjected to higher fatigue damage for large H_s (in the order of 10^{-4}) than line 1 and 2 (ranging in the order of 10^{-5}).

4.3. Fatigue prediction

When combined with a suitable wave scatter plot, the individual fatigue damage values can be aggregated to an annual or long-term fatigue damage estimate, see equ. 8 and 9. The question of how suitable different wave climates are was addressed in section 4.1. For this case study 2 estimates are presented:

1. Observed wave climate
2. Modelled long-term hindcast wave climate

   Based on the comparison of modelled and measured wave parameters the modelled hindcast wave period is adjusted by 2s, i.e. the scatter plot is shifted to the right by one column. This is justified by the

observed under prediction of T_P in the hindcast by 2s compared to the measured conditions as identified in sec. 4.1, see fig. 9 and 10. Essentially this adjustment is a calibration of the model output against the measured field data. A detailed overview of calibration techniques to remove data trends in wave measurements is presented by Mackay et al. (2010).

Furthermore, three cells in the adjusted scatter plot do not have a counterpart in the measured data set. The probabilities of these cells have been added to the nearest neighbour cells:

$$(H_s, T_p) = (3 - 3.5, 8 - 12) = 1.5\% \mapsto (2.5 - 3; 8 - 10); \tag{10}$$

$$(2 - 2.5, 8 - 10) = 0.8\% \mapsto (2 - 2.5; 8 - 10) \tag{11}$$

This adjustment applies only to 2.3% occurrence probability for the entire year and is deemed acceptable in this case as the introduced deviation in wave height is small. As the 1.5% occurrence probability of $H_s = [3 - 3.5m]$ is assigned to $H_s = [2.5 - 3m]$ a slightly less conservative fatigue estimate should be expected.

The annual accumulated fatigue damage for the individual mooring lines in the case of the modelled and measured wave climate conditions is summarised in table 5. As expected, the chain in mooring line three experiences the largest fatigue damage in both instances as it showed the highest damage for the individual sea states. It is noteworthy that the difference in fatigue damage between the mooring lines in this spread configuration is a factor of 1:5 (L3:L2) and almost 1:12 (L3:L1), due to unequal loading caused by the mean wave and wind direction and the resulting motion response of the buoy. In comparison, the disparity introduced by the different wave climates is in the order of 50%, i.e. amounts to a factor

Table 5: Annual accumulated fatigue damage estimates based on measured and modelled wave climate

Line	Measured	Modelled	Difference [%]
L1	$1.93 \cdot 10^{-3}$	$2.99 \cdot 10^{-3}$	-55
L2	$4.42 \cdot 10^{-3}$	$6.92 \cdot 10^{-3}$	-56
L3	$2.29 \cdot 10^{-2}$	$3.40 \cdot 10^{-2}$	-49

of 2.

For mooring line three, the estimated annual accumulated fatigue damage is depicted in figure 14. The contour plot has been derived through interpolation from the discrete data points of the scatter plot. It facilitates the legibility and accounts for the fact that real sea conditions are of a continuous rather than discrete nature. The colour scheme that characterises the fatigue level is equal for both the measured and modelled case. The hindcast wave climate, fig. 14(b), yields higher fatigue levels and a higher accumulated fatigue damage D compared to the measured wave conditions, fig. 14(a). Yet, the shape of the contours resemble each other in that the highest fatigue damage occurs in the region of $H_s = 2m$ with $T_p = 6 - 8s$. As a result, the specific site conditions and the associated fatigue damage levels are considered to be modelled and characterised to a good level of agreement between long-term hindcast and field measurements.

5. Discussion

The results are put into context with a view on the safety factors of the presented case study as well as the sea state and load measurements for the

fatigue assessment and prediction.

The validity of the fatigue damage predictions cannot be assessed here, as damage predictions can only be compared with S-N data from a DNV guidance document for mooring line materials. Validation of the fatigue damage predictions can be best achieved through experimental tests that replicate the operational loads (Thies et al., 2011) and recent tests reported by Fredheim et al. (2013) indeed suggest very good agreement of S-N curves and cycles to failure under experimental conditions for offshore mooring chain.

5.1. Effect of mean stress on fatigue life

The fatigue curves used for the damage accumulation assume a completely reversed load amplitude with a mean stress $\sigma_m = 0$. Thus, the effects of mean stress on the mooring line fatigue have not been considered so far. It is well known that an increased mean stress reduces the fatigue life of the component under loading. Commonly used relationships to model the mean stress effect, such as the Gerber parabola, Goodman line and Soderberg curve, calculate an adjustment factor to decrease the stress amplitude at zero men stress $sigma_e$ to the amplitude under mean stress σ_a for a given number of load cycles N (Campbell, 2008, p. 246):

$$\frac{\sigma_a}{\sigma e} = 1 - (\frac{\sigma_m}{\sigma_u})^z \tag{12}$$

where $z = 1$ for the Goodman line and Soderberg curve, $z = 2$ for the Gerber curve, $\sigma_u = \sigma_y$ for the Soderberg curve, and σ_e is the fatigue limit for completely reversed bending.

The Gerber parabola is the least conservative adjustment, while the Goodman line is often used in practice to accommodate the scatter of fa-

Table 6: Adjustment factors for mean stress effect, ratio of stress amplitude under mean stress σ_a and stress amplitude under fully reversed bending,σ_e; $\frac{\sigma_a}{\sigma_e}$.

Method	Line 1	Line 2	Line 3
Gerber	1	1	1
Goodman	0.995	0.993	0.994
Soderberg	0.990	0.988	0.989

tigue data. For design based on the yield strength rather than the ultimate strength the more conservative Soderberg curve applies.

In the presented case study the mean stresses of the mooring lines (24mm open link riser chain) are $\sigma_{m,\,L1} = 2.58MPa$; $\sigma_{m,\,L2} = 3.37MPa$; $\sigma_{m,\,L1} = 2.91MPa$. The associated yield and ultimate stress of the chain are supplied by the manufacturer load test as: $\sigma_y = 270.7MPa$ and $\sigma_u = 505.8MPa$. The calculations after equation 12 give the values summarised in table 6. The Gerber parobola yields a negligible effect while the Soderberg curve demands an adjustment of only 1.2% ($\frac{\sigma_a}{\sigma_e} = 0.988$).

Thus, for the presented case study, the mean stress in the mooring lines is too small to significantly affect the fatigue life. However, the mean stress may play a more considerable role for systems with higher pre-tensions. As an example, for the Oscillating Water Column device specified in Ferrario et al. (2004) a 114mm chain was pre-tensioned with 90 tonnes. The effect of mean stress on the fatigue life was not considered in, but is more significant with factors for the mean stress effect between $\frac{\sigma_a}{\sigma_e} = 0.845$ (Soderberg-curve) and $\frac{\sigma_a}{\sigma_e} = 0.993$ (Gerber-parabola).

5.2. Safety factors

The safety factor for fatigue considerations is usually calculated as the ratio between determined fatigue life and the desired design life of a component/structure. Table 7 summarises the computed fatigue life together with the associated safety factors. The fatigue life is the reciprocal value of the fatigue damage, i.e. $L_{Fatigue} = \frac{1}{D_{annual}}$, while the safety factor S_{Life} is the ratio of fatigue life and design life, $S_{Life} = \frac{L_{Fatigue}}{L_{Design}}$. As a demonstration test installation, the design life of the SWMTF is five years, while typical project life times for for a MEC installation is expected to be at least 20 years.

Considering the safety factor with regards to design life S_{Life}, a wide spread of values is recognised, ranging from a safety factor of over 100 for the measured conditions of mooring line 1 to a safety factor of 6 for mooring line 3 under modelled wave conditions.

The single safety factor for the fatigue limit state (FLS), γ_f, stated in the Offshore Position Mooring Standard DNV-OS-E301 (2010) is $\gamma_f = 5$, for conditions where mooring lines are not regularly inspected onshore and the accumulated damage is $D \leq 0.8$. Hence, the fatigue design for line three complies with the standard and is well met for all other mooring lines, too.

If the loads cannot be predicted with confidence as it is the case for marine environments with large inter annual variations of wave conditions and highly dynamic motion responses, one should also consider a safety factor with regard to mooring line forces.

Assuming a safety factor of 2 would be desirable regarding mooring forces it would allow for a doubling of mooring forces and thus a doubling

Table 7: Fatigue life and safety factors regarding design life and force uncertainty

	Measured			Modelled		
	L1	L2	L3	L1	L2	L3
Fatigue life $L_{Fatigue}$	517	226	44	334	145	29
Safety factor (Design Life 5 years) S_{Life}	103	45	9	67	29	6
Safety factor (Force increase factor 2) S_{Force}	8	6	3.5	7	5	3

of component stresses. The effect an increased stress range has on the fatigue life can be estimated through the S-N curve (equ. 3), where the parameter β describes the slope of the curve. For different materials, β typically ranges between values of 3 and 5, with the presented studless chain being $\beta_{chain,\ studless} = 3$ (see fig. 7). Thus, a load increase by a factor of 2 would increase the fatigue damage D by a factor of $2^3 = 8$. In other words, if a safety factor of 2 towards mooring forces is desired, the safety factor towards fatigue life would have to be 8. It is noteworthy that for higher values of β the fatigue life safety factor would also be higher. For example spiral steel wire rope is characterised by $\beta = 4.8$, which leads to a factor of $2^{4.8} \approx 28$ as a required fatigue life safety factor.

The presented analysis only considered the riser chain. Another issue which is likely to impact the fatigue life of mooring systems in shallower water are abrasion effects for the bottom chain which is in contact with the seabed. Beside the area that experiences repeated lift and touchdown, the sea bed will be disturbed by longer period waves which may create a gritty emulsion, in particular if sand is present, which would cause abrasion damage between the chain links and thus reduce the fatigue life.

5.3. Sea state and load measurements

Scatter plots are classified through bins (typically H_s interval of $0.5m$ and T_p interval of $1s$) and thus are a simplification of the actual occurring wave conditions. Resolution may be improved if bins are reduced, however, an increased resolution will make it more difficult to populate all scatter bins during field deployment tests.

For the presented case study, the wave scatter plot of the modelled annual wave climate did not have counterparts for the load measurement in all situations. Therefore, the probability of unpopulated cells was migrated to cells where load information was available. This approach becomes less feasible the more cells are not populated with load information. In such cases, either data from experimental or numerical modelling should be sought to inform the load behaviour. Thies et al. (2012) have estimated the fatigue damage with a limited number of tank test sea states but had to relate the fatigue damage to the wave height only which introduces further uncertainties toward the fatigue estimate. Extensive field measurements would be preferable over numerical or experimental load data. However, the analyst is usually constraint by a limited amount of load information. This is particularly the case in early design stages where the cost implications of field tests are often prohibitively high in comparison to numerical models.

It is further important to assess the contribution the individual sea state conditions make to the accumulated fatigue damage. The hindcast model presented earlier could not describe small wave height, high period wave conditions which have been measured during the deployment. However, as was shown in figures 11-13 these small sea states have a negligible effect

on the fatigue damage. Conversely, the modelled, but not measured larger sea states with $H_s = 3 - 3.5m$ have a more significant effect on the fatigue damage. They have been indirectly accounted for through conditions with $H_s = 2.5 - 3m$, but will ideally be measured in future deployments.

With regard to the sea state prediction and estimation of extreme events, the gathered wave measurements will be used to calibrate the numerical wave model for the location based on recorded wind field data. If a satisfactory correlation can be obtained, the numerical model may be used to compensate any missing wave measurements and to predict the long term extreme sea states with confidence.

6. Conclusion

The reported results are the first published account of extensive field load measurements for floating marine energy conversion systems. As such, they bear wider implications for the design, site assessment and load monitoring of marine energy devices. This paper has demonstrated a methodology to estimate and predict the fatigue life and associated safety factors from field load measurements. A key result for the analysed SWMTF installation is that the fatigue loading of mooring lines can differ by more than an order of magnitude, as it is the case for the investigated spread mooring configuration. This raises a twofold concern for marine energy mooring systems. On the one hand the system must be designed to withstand the fatigue limit state with confidence, yet a safety factor of more than $S_{Life} > 10$ must be regarded as overly conservative design which carries unnecessary cost.

It was shown that in a spread mooring system the different lines are likely to carry different loads dependent on the main wind- and wave directions. This question is important for a site-specific and lean design and will require good directional wave spectra for prospective sites. If the leading, seaward, mooring lines are designed to withstand higher loads than the rear mooring lines, consideration must be given during the design and performance prediction stage to how the dynamic response of the coupled system is affected.

Another reason that advocates the detailed measurement and modelling of all anticipated load cases was found in the stress safety factor. It was shown that through the S-N curve relationship, any uncertainty in the load case will translate exponentially to the required fatigue life safety factor. To put it optimistically, any reduction of load uncertainties will reap an exponential benefit in the fatigue design.

In order to emphasise the importance of careful fatigue assessment for marine renewable energy systems, it must also be noted here that the presented case is located at a relatively sheltered site. The calculated fatigue damage is observed to be directly proportional to wave height, but the fatigue damage induced by more extreme sea states cannot be easily extrapolated to higher sea states. As such, the presented fatigue life cannot be simply transferred to real wave energy converter which would typically be deployed in a more exposed site with higher wave energy levels. At commercial demonstration sites, such as the Wave Hub, the mooring system will have to regularly withstand more extreme sea states. At Wave Hub, signif-

icant wave heights reach over $H_s = 6m$, rather than $H_s = 3m$ as presented in this paper.

However, the presented approach to use field measurements to assess the fatigue life of components can be transferred to full-scale applications. Beyond this, the extrapolation of fatigue damage contributions during higher sea states can be achieved through carefully calibrated hydrodynamic numerical models. For fatigue evaluation purposes field measurements would be preferable as the modelling uncertainty of load conditions is removed. As a consequence, it should be a priority during the development stage to gather as much field load information as possible and to establish 'load libraries' which assist the design teams in the fatigue estimation and subsequent design improvement for future deployments. Continuous load monitoring during the deployment will also ensure that the fatigue capacity of the mooring system is not reached and makes timely intervention possible if a mooring line should be at the risk of fatigue failure.

Acknowledgements

The authors would like to acknowledge the support of the UK Centre for Marine Energy Research (UKCMER) under the SuperGen marine programme funded by the Engineering and Physical Sciences Research Council (EPSRC), grant EP/I027912/1 (www.supergen-marine.org.uk). The authors also acknowledge the support of the MERiFIC project partners (Marine Energy in Far Peripheral and Island Communities, http://www.merific.eu).

This research has also received support from MARINET, a European Community - Research Infrastructure Action under the FP7 Capacities Spe-

cific Programme (www.fp7-marinet.eu). The authors are also grateful for the valuable comments of Prof Julian Wolfram during the review of this paper and for the work of Baptiste Chardon who assisted with some of the data processing during an internship at the University of Exeter.

BVG Associates, 2011. Wave and tidal energy in the Pentland Firth and Orkney waters: How the projects could be built. Technical Report. The Crown Estate. A report commissioned by The Crown Estate and prepared by BVG Associates.

Campbell, E. (Ed.), 2008. Elements of Metallurgy and Engineering Alloys. Asm International. chapter 14 Fatigue. pp. 243–264.

Cui, W., 2002. A state-of-the-art review on fatigue life prediction methods for metal structures. Journal of Marine Science and Technology 7, 43–56.

Dalton, G., Alcorn, R., Lewis, T., 2012. A 10 year installation program for wave energy in ireland: A case study sensitivity analysis on financial returns. Renewable Energy 40, 80 – 89. doi:10.1016/j.renene.2011.09.025.

DNV-OS-E301, 2010. Offshore standard - Position Mooring. Standard. Det Norske Veritas [DNV].

EMEC, 2011a. Full scale prototype testing. Technical Report. European Marine Energy Centre EMEC. URL: `www.emec.org.uk`.

EMEC, 2011b. Nursery facilities for scale testing. Technical Report. European Marine Energy Centre. URL: `www.emec.org.uk`.

FaB Test, 2011. Falmouth Bay Test Site, Marine renewables comissioning site. Description of Site Characteristics and Eligible Test Installations. Technical Report FHC / FT / 104 (issue 1). Falmouth Harbour commissioners and University of Exeter.

Ferrario, S., King, D., Gould, J., 2004. The technical challenges in designing, building and installing a moored wave energy device at Port Kembla, New South Wales. Technical Report. J P Kenny.

Fitzgerald, J., Bergdahl, L., 2008. Including moorings in the assessment of a generic offshore wave energy converter: A frequency domain approach. Marine Structures 21, 23–46.

FORCE, 2012. Force test site. URL: `http://fundyforce.ca/testsite`.

Fredheim, S., Reinholdtsen, S.A., Håaskoll, L., Lie, H.B., 2013. Corrosion fatigue testing of used, studless offshore mooring chains, in: Proc. of 32nd Int. Conf. on Ocean, Offshore and Arctic Engineering, ASME, Nantes, France.

Golding, B., 1983. A wave prediction system for realtime sea state forecasting. Quarterly Journal of the Royal Meteorological Society 109, 393–416.

Harnois, V., Johanning, L., Thies, P.R., Bjerke, I., under review. The influence of environmental conditions on the extreme mooring loads for highly dynamic responding moored structures. Ocean Engineering .

Harnois, V., Parish, D., Johanning, L., 2012. Physical measurement of a slow drag of a drag embedment anchor during sea trials, in: 4th International Conference on Ocean Energy, Dublin, Ireland.

Johanning, L., Smith, G.H., Wolfram, J., 2005. Towards design standards for wec moorings, in: Proc. European Wave and Tidal Energy Conference (EWTEC), Glasgow.

Johanning, L., Smith, G.H., Wolfram, J., 2006. Mooring design approach for wave energy converters. Proceedings of the Institution of Mechanical Engineers, Part M: Journal of Engineering for the Maritime Environment 220, 159–174. doi:10.1243/14750902JEME54.

Johanning, L., Smith, G.H., Wolfram, J., 2007. Measurements of static and dynamic mooring line damping and their importance for floating wec devices. Ocean Engineering 34, 1918 – 1934. doi:10.1016/j.oceaneng.2007.04.002.

Johanning, L., Thies, P.R., Parish, D., Smith, G.H., 2011. Offshore reliability approach for floating renewable energy devices, in: Proc. of 30th Int. Conference on Ocean, Offshore and Arctic Engineering OMAE, Rotterdam, Netherlands.

Leijon, M., Bostrm, C., Danielsson, O., Gustafsson, S., Haikonen, K., Langhamer, O., Strmstedt, E., Stlberg, M., Sundberg, J., Svensson, O., Tyrberg, S., Waters, R., 2008. Wave energy from the north sea: Experiences from the lysekil research site. Surveys in Geophysics 29, 221–240. doi:10.1007/s10712-008-9047-x.

Mackay, E.B., Bahaj, A.S., Challenor, P.G., 2010. Uncertainty in wave energy resource assessment. part 1: Historic data. Renewable Energy 35, 1792 – 1808. doi:http://dx.doi.org/10.1016/j.renene.2009.10.026.

Mora-Figueroa, V.O., Olivares, C., Holmes, B., O'Hagan, A., 2012. Catalogue of Wave Energy Test Centres. Technical Report Deliverable D2.1, Grant Nr. IEE/09/809/SI2.558291. Streamlining of Ocean Wave Farms Impact Assessment (SOWFIA).

Mouslim, H., Babarit, A., Clment, A., Borgarino, B., 2009. Development of the french wave energy test site sem-rev, in: Proc. 8th European Wave and Tidal Energy Conference (EWTEC), pp. 31–35.

Mueller, M., Jeffrey, H., Wallace, R., von Jouanne, A., 2010. Centers for

marine renewable energy in europe and north america. Oceanography 23, 42–52.

van Nieuwkoop, J.C., Smith, H.C., Smith, G.H., Johanning, L., 2013. Wave resource assessment along the cornish coast (uk) from a 23-year hindcast dataset validated against buoy measurements. Renewable Energy 58, 1–14. doi:http://dx.doi.org/10.1016/j.renene.2013.02.033.

Nijssen, R.P.L., 2006. Fatigue life prediction and strength degradation of wind turbine rotor blade composites. Contractor report sand2006-7810p, sandia national laboratories. Delft University of Technology.

Palha, A., Mendes, L., Fortes, C.J., Brito-Melo, A., Sarmento, A., 2010. The impact of wave energy farms in the shoreline wave climate: Portuguese pilot zone case study using pelamis energy wave devices. Renewable Energy 35, 62 – 77. URL: http://www.sciencedirect.com/science/article/pii/S0960148109002687, doi:10.1016/j.renene.2009.05.025.

Rychlik, I., 1987. A new definition of the rainflow cycle counting method. Int. Journal of Fatigue 9, 119–121.

Schijve, J., 2009. Fatigue of structures and materials. Springer.

Schütz, W., 1996. A history of fatigue. Engineering Fracture Mechanics 54, 263 – 300. URL: http://www.sciencedirect.com/science/article/pii/0013794495001786, doi:10.1016/0013-7944(95)00178-6.

Stacey, A., Sharp, J.V., 2007. Safety factor requirements for the offshore industry. Engineering Failure Analysis 14, 442 – 458.

SWRDA, 2011. Invitation to express an interest in deploying at Wave Hub in 2012. www.wavehub.co.uk. South West Regional Development Agency, accessed on 28/12/2011.

Thies, P.R., Johanning, L., Smith, G.H., 2011. Towards component reliability testing for marine energy converters. Ocean Engineering 38, 360 – 370. URL: http://www.sciencedirect.com/science/article/B6V4F-51R51K6-1/2/3923dc818c4107b6d doi:DOI: 10.1016/j.oceaneng.2010.11.011.

Thies, P.R., Johanning, L., Smith, G.H., 2012. Lifecycle fatigue load spectrum estimation for mooring lines of a floating marine energy converter, in: 31st Int. Conference on Ocean, Offshore and Arctic Engineering OMAE, American Society of Mechanical Engineers ASME, Rio De Janeiro, Brazil.

WAFO-group, 2000. WAFO - A Matlab Toolbox for Analysis of Random Waves and Loads - A Tutorial. Center for Math. Sci., Lund Univ. Lund, Sweden.

Wang, K.S., Shen, Y.C., Huang, J., 1997. Loading adjustment for fatigue problem based on reliability considerations. International Journal of Fatigue 19, 693 – 702.

List of Figures

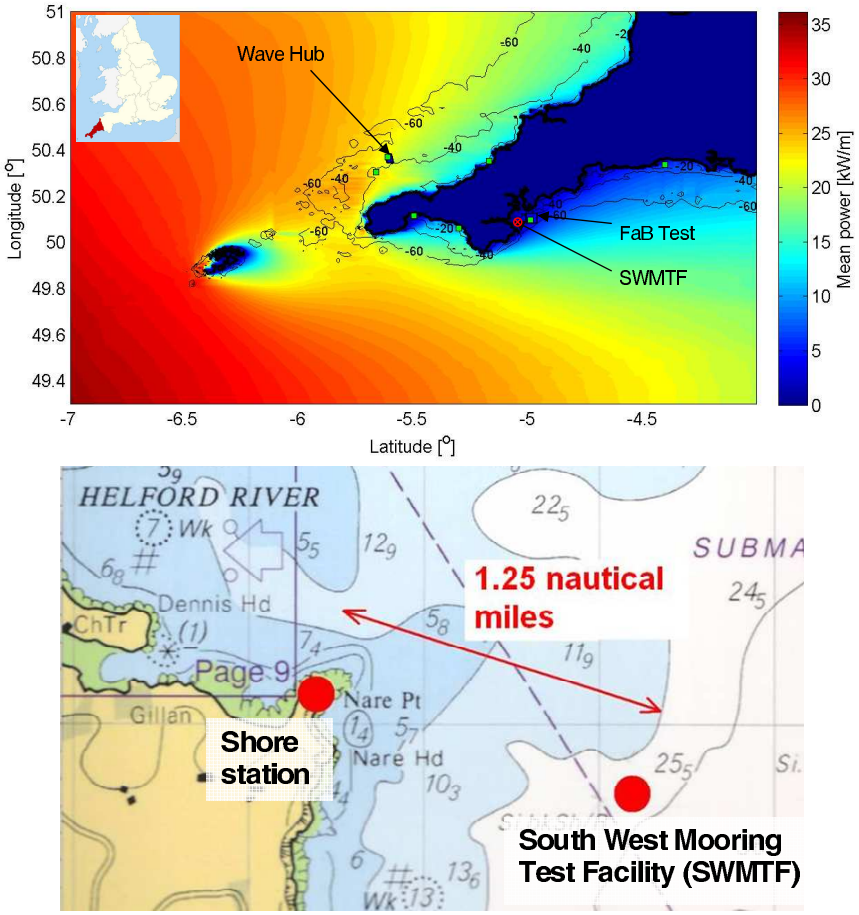

Figure 1: Location of South West Mooring Test Facility (SWMTF), showing mean wave power levels and bathymetry contours for the Cornish coast, adapted after van Nieuwkoop et al. (2013)

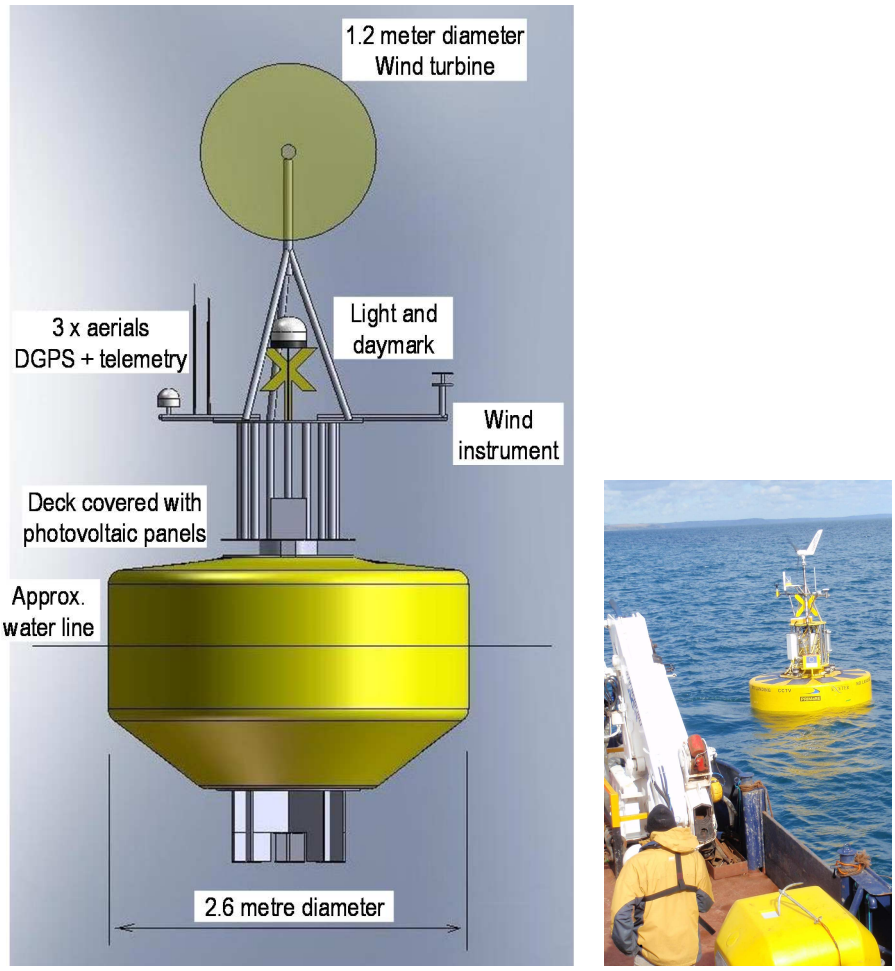

(a) Drawing (b) Installed

Figure 2: South West Mooring Test Facility Buoy

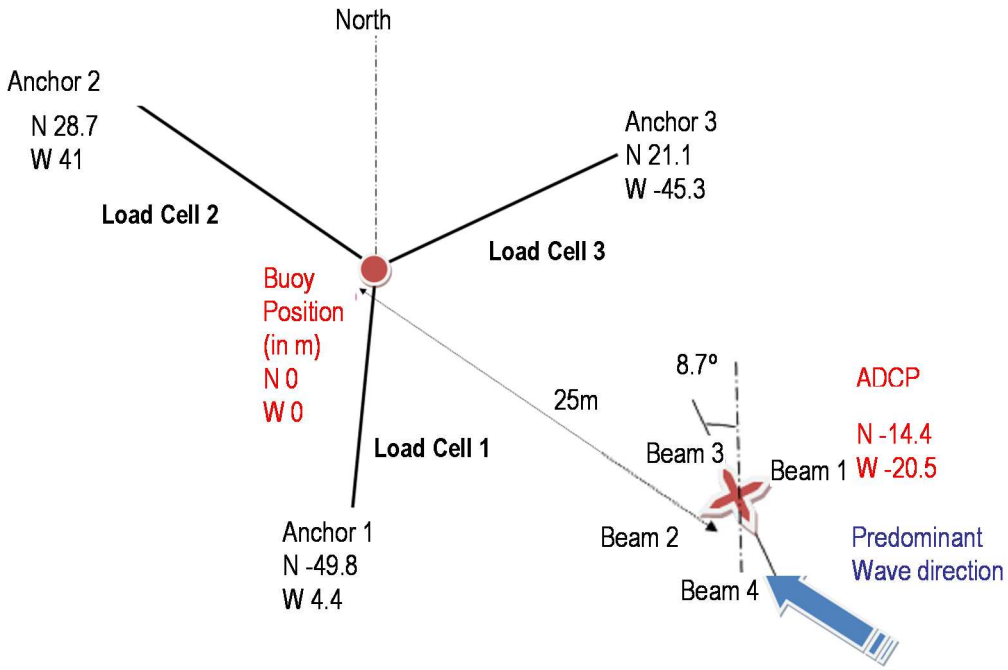

Figure 3: Schematic drawing of mooring configuration (plan view)

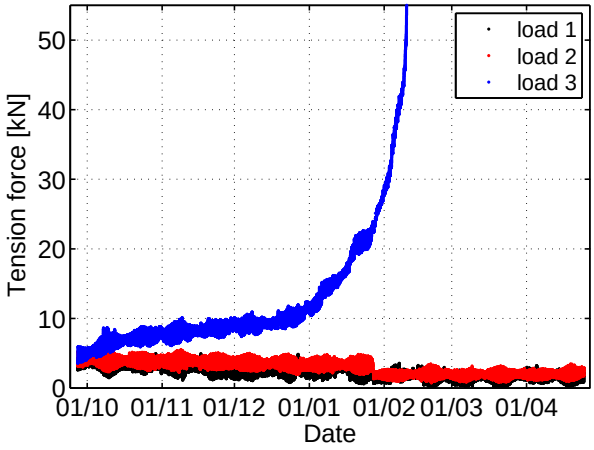

(a) Raw data

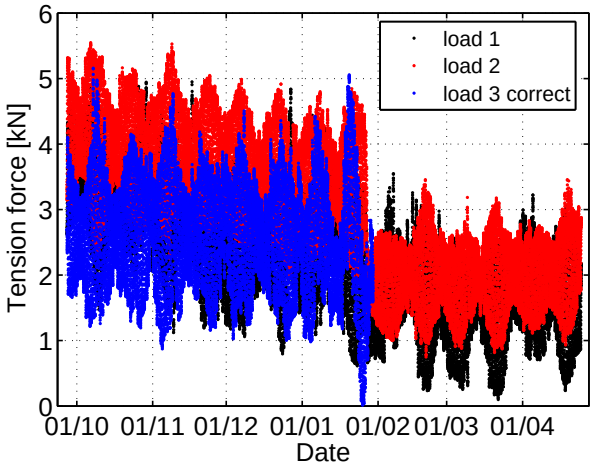

(b) Corrected

Figure 4: Mean mooring line tension force of individual 10min files measured during SWMTF deployment, 4(a), and corrected for load cell drift in line 3, 4(b).

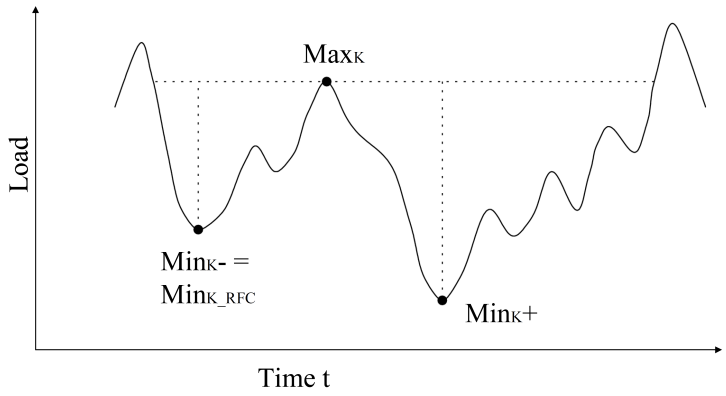

Figure 5: Rainflow cycle count definition (after Rychlik, 1987)

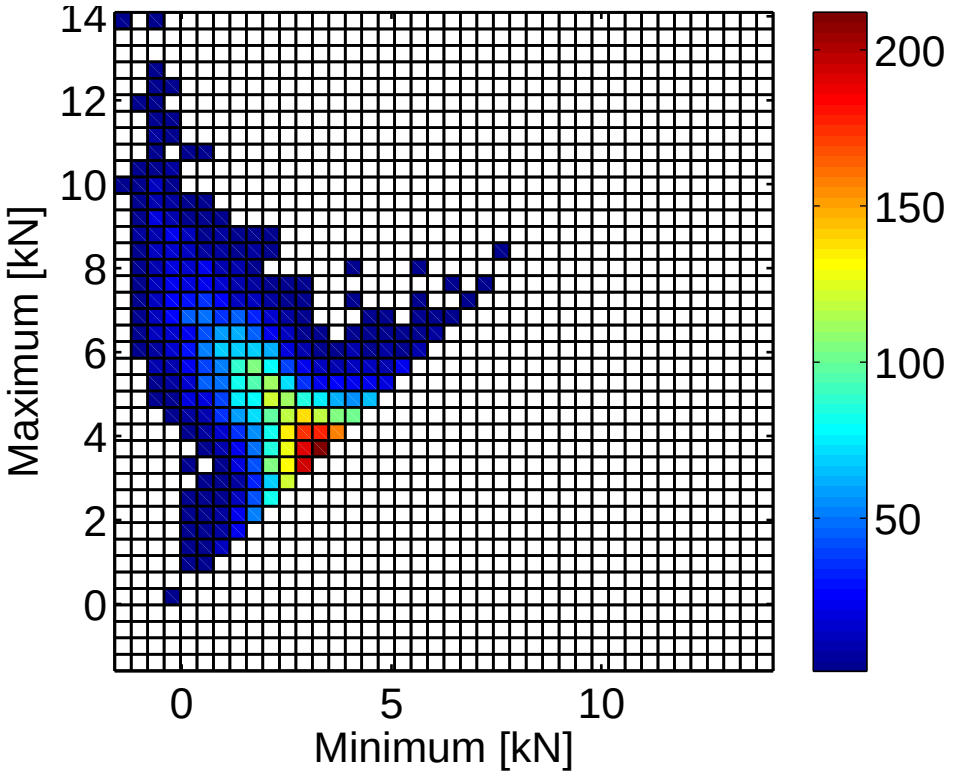

Figure 6: Rainflow matrix for mooring line 2 in typical moderate sea state, $H_s = 2-2.5$m; $T_p = 8-10$s.

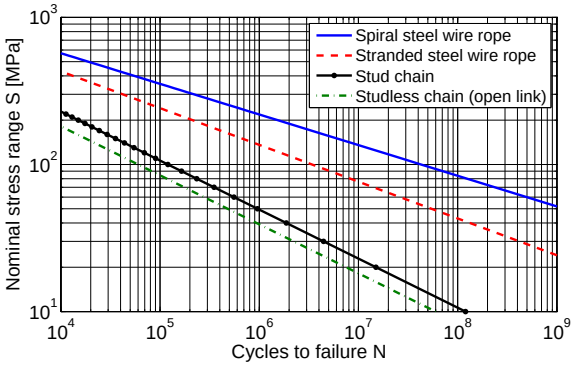

Parameters

Type	K	β
Spiral	$1.7 \cdot 10^{17}$	4.8
Stranded	$3.4 \cdot 10^{14}$	4.0
Stud	$1.2 \cdot 10^{11}$	3.0
Studless	$6.0 \cdot 10^{10}$	3.0

Parameters shown for: $log\,(N(S)) = log\,(K) - \beta \cdot log\,(S)$

Figure 7: Nominal S-N fatigue curves for mooring materials, after DNV-OS-E301 (2010).

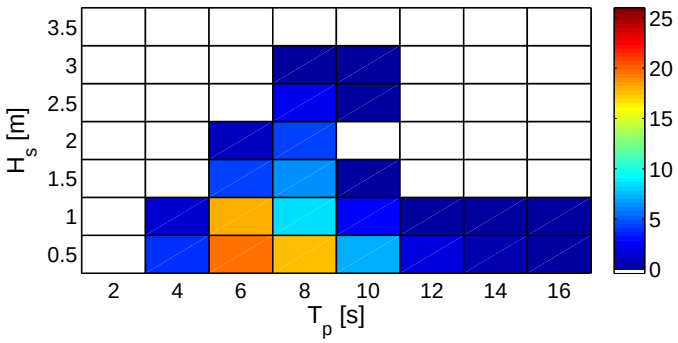

(a) Measured

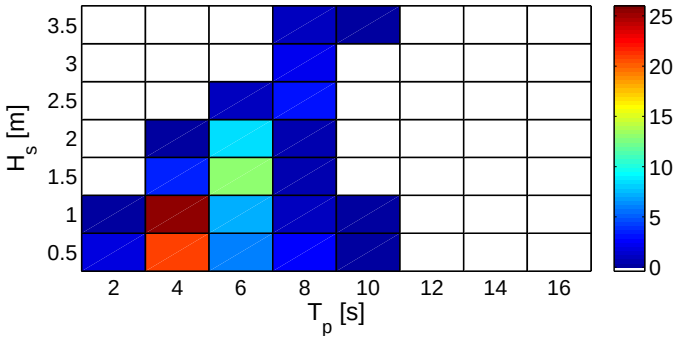

(b) Hindcast

Figure 8: Scatter plot of measured and modelled sea states. Colour denotes the percentage occurrence.

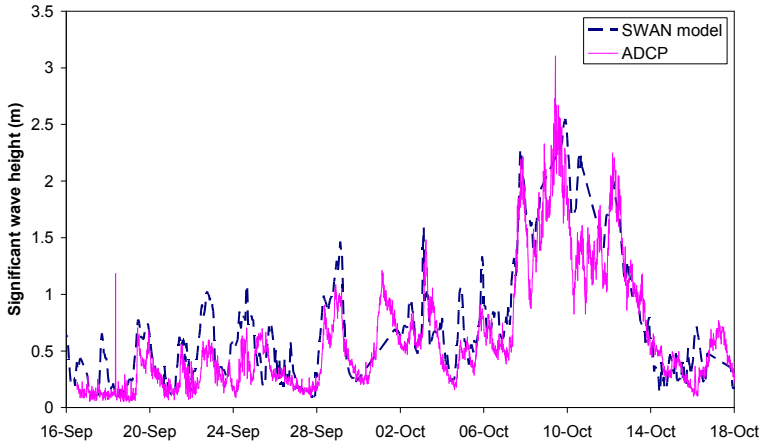

(a) Significant Wave heigh H_s

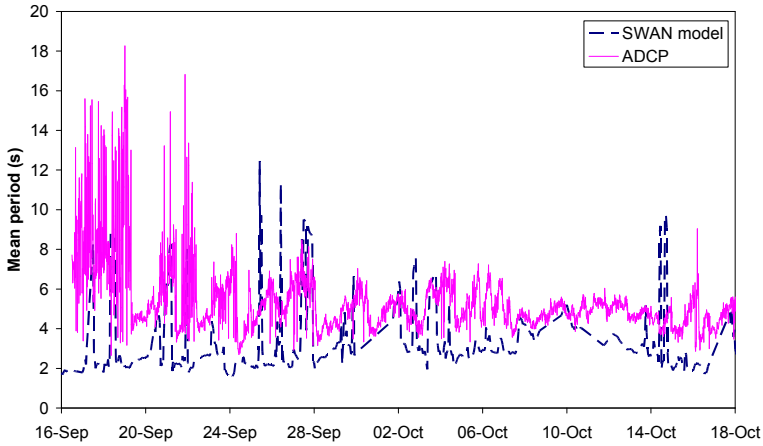

(b) Mean period T_{m02}

Figure 9: Comparison between SWAN model output and ADCP measurements at SWMTF site, measured in 2010.

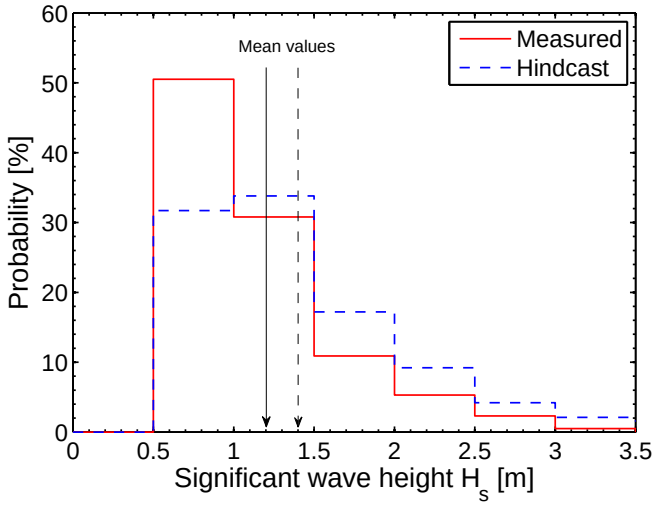

(a) Measured

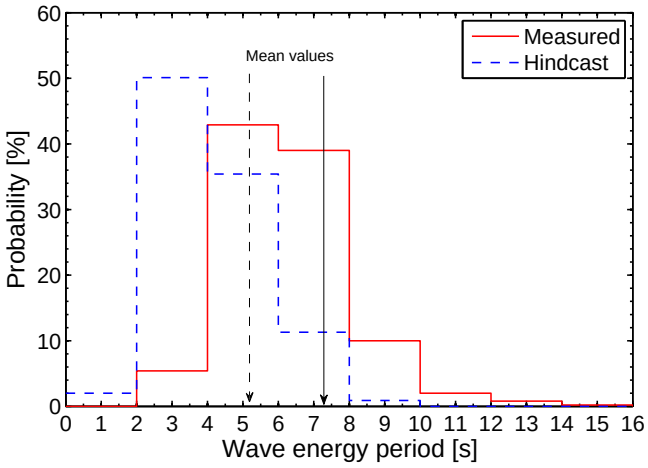

(b) Hindcast

Figure 10: Comparison of measured and modelled wave climate parameter distributions for SWMTF site, arrows indicate mean values

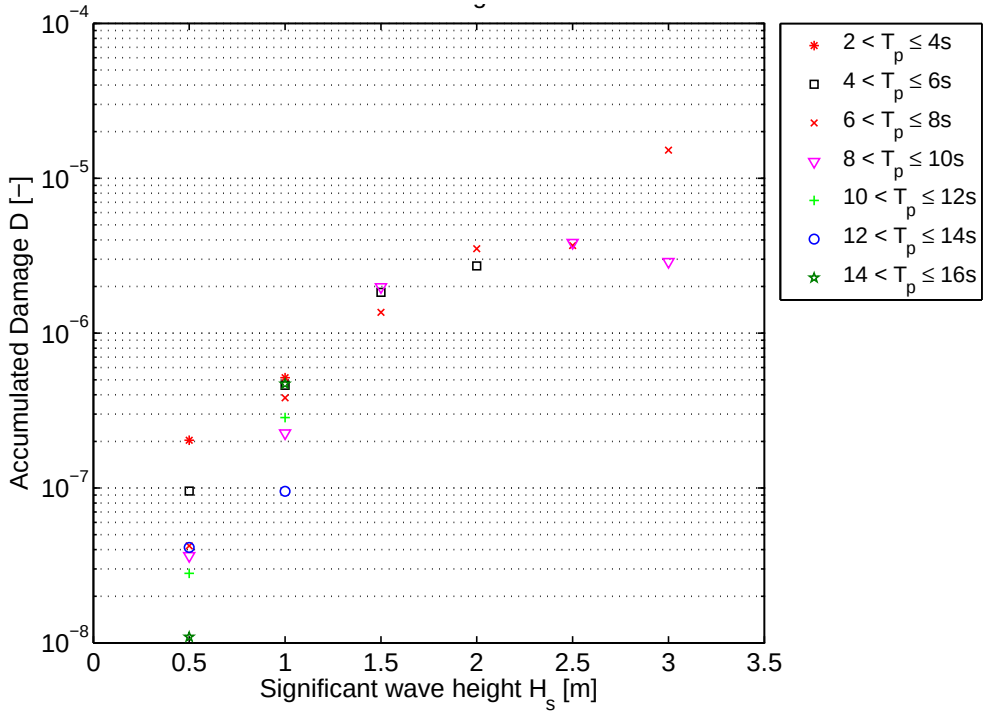

Figure 11: Mooring line 1 fatigue damage of individual sea states for open link riser chain ($d = 24mm$).

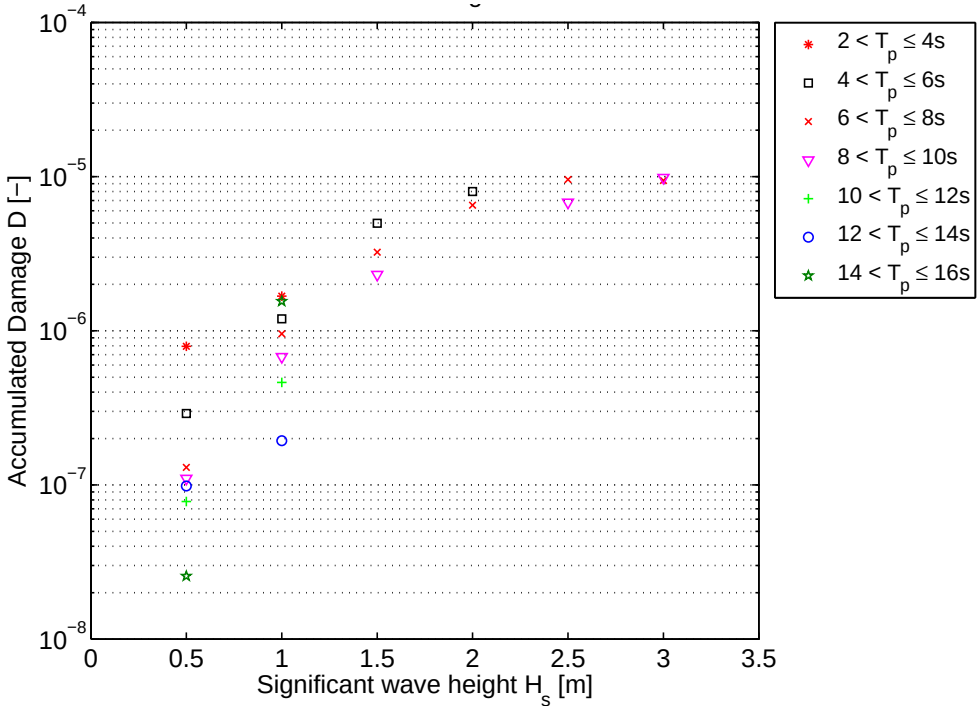

Figure 12: Mooring line 2 fatigue damage

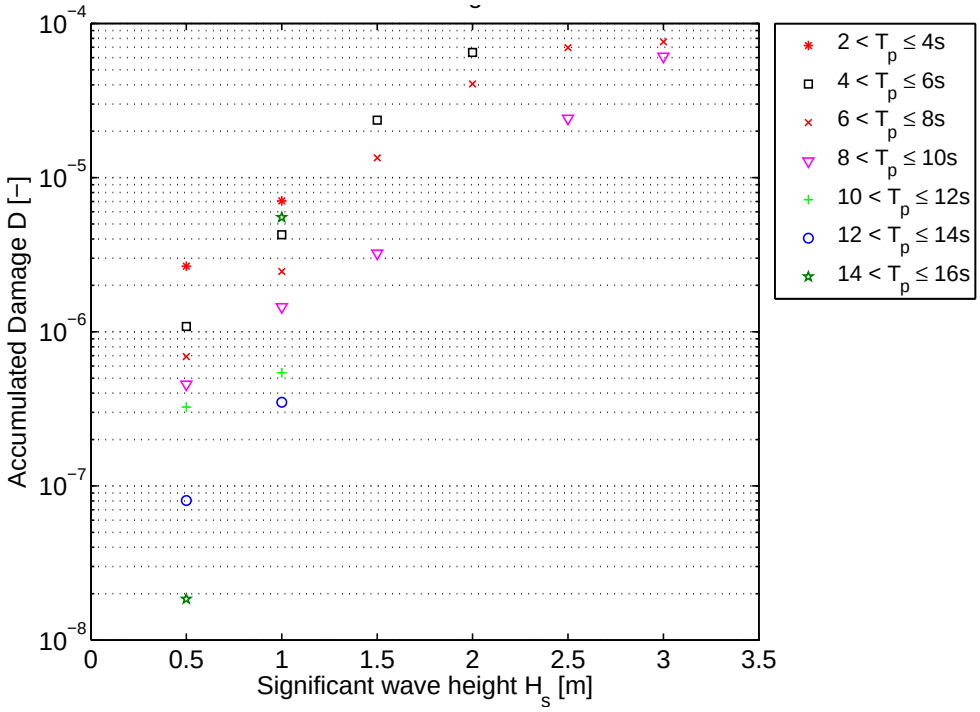

Figure 13: Mooring line 3 fatigue damage

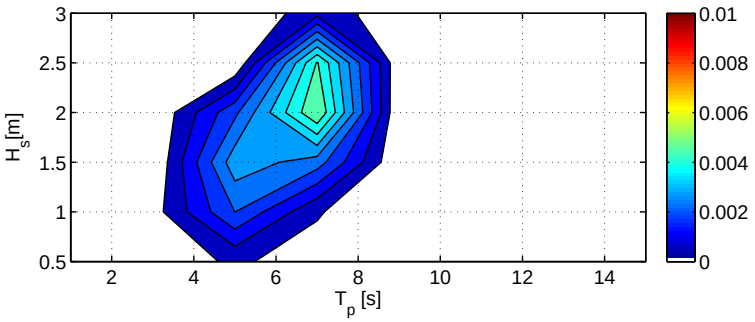

(a) Measured, $D = 2.29 \cdot 10^{-2}$

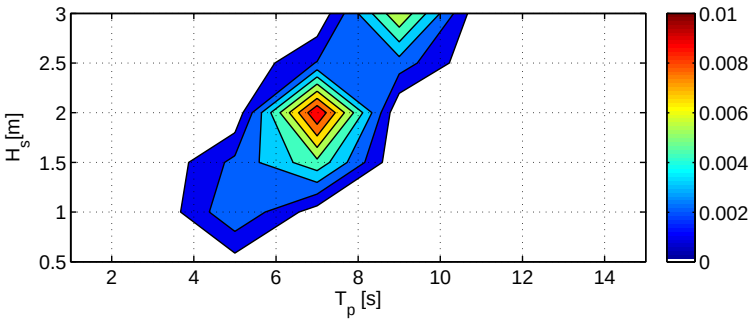

(b) Hindcast $D = 3.40 \cdot 10^{-2}$

Figure 14: Contour plot of annual accumulated fatigue damage for mooring line 3, with measured and modelled wave climate parameters. D denotes accumulated fatigue damage for one year, colour shows fatigue damage.